GEOPHYSICAL RESEARCH LETTERS, VOL. ???, XXXX, DOI:10.1029/,

Climate Response to a Geoengineered Brightening of Subtropical Marine Stratocumulus Clouds

Spencer Hill[1] and Yi Ming[2]

Spencer Hill, Program in Atmospheric and Oceanic Sciences, Princeton University, Princeton, NJ 08540, USA. (spencerh@princeton.edu)

Yi Ming, Geophysical Fluid Dynamics Laboratory/NOAA, Princeton, NJ 08540, USA. (Yi.Ming@noaa.gov)

[1]Program in Atmospheric and Oceanic Sciences, Princeton University, Princeton, NJ

[2]Geophysical Fluid Dynamics Laboratory/NOAA, Princeton, NJ

As a means of mitigating anthropogenic climate change, there have been suggestions to increase the albedo of low-level marine clouds through the aerosol indirect effects by deliberately injecting them with sea salt. However, the full climate response to this geoengineering scheme is currently poorly understood. We simulate cloud seeding in a coupled mixed-layer ocean-atmosphere general circulation model in order to identify the specific physical mechanisms through which seeding could operate. Seeding stratocumulus decks over three subtropical maritime regions produces strong local radiative deficits, both due to enhancement of the local cloud albedo and direct scattering of solar radiation by the added sea salt aerosols. Though the resulting cooling is fairly well spread over most of the globe, differential cooling over the equatorial Pacific Ocean induces a La Niña-like climate response, with tropical precipitation changes resembling La Niña anomalies and teleconnections occuring in the North Pacific. Additionally, model runs in which only one of the three regions is seeded indicate some nonlinearity in the climate response. We identify dynamical and thermodynamical constraints respectively on the temperature and hydrological cycle responses to cloud seeding, but the full response to such geoengineering remains poorly constrained.

1. Introduction

Enhancing the albedo and lifetime of marine boundary layer clouds by deliberately injecting them with sea salt aerosols has previously been proposed as a geoengineering method of mitigating temperature rise due to anthropogenic climate change [*Latham*, 1990, 2002]. The added aerosols would act as cloud condensation nuclei, thereby inducing local cooling through the aerosol indirect effects. Initial model studies have suggested that such a cloud seeding scheme could effectively enhance the albedo of subtropical marine stratocumulus decks [*Latham et al.*, 2008] and that, if deployed at sufficiently large scale, could offset a significant fraction of the projected global warming [*Latham et al.*, 2008; *Jones et al.*, 2009; *Rasch et al.*, 2009]. These results must be taken in context, however, that the aerosol indirect effects are poorly understood [e.g. *Lohmann et al.*, 2010].

In addition to its intended result of minimizing global-mean temperature rise, cloud seeding would also produce unintended consequences, that is, changes to the climate that could be deleterious to human society and/or ecosystems. Alterations of local to regional precipitation patterns are of particular concern in this respect, which presents a considerable challenge given the difficulty of accurately resolving precipitation on these scales in current generation coarse-resolution climate models. Accurately constraining these unintended consequences therefore requires a solid theoretical understanding of the full climate response to cloud seeding.

This full response, however, has only just begun to be explored, with only a few general circulation model (GCM) studies published to date. Using a coupled atmosphere-ocean GCM (AOGCM), *Jones et al.* [2009] (hereafter referred to as J09) increased cloud droplet number concentration (N_d) to 375 cm^{-3} over three subtropical marine regions (Fig. 1 of J09) in addition to A1B emissions scenario greenhouse gas forcing. *Rasch et al.* [2009] (hereafter referred to as R09) imposed both doubled CO_2 forcing (710 ppmv CO_2) and increased N_d to 1000 cm^{-3} between 850 and 1000 hPa over fixed percentages of the ocean surface (20, 30, 40, or 70% of total ocean area) in a series of AOGCM experiments, with seeding locations varying in time according to the location of the most susceptible clouds.

In the present study, we use an atmosphere general circulation model (AGCM) coupled to a mixed-layer ocean model to simulate the climate impacts of cloud seeding. After analyzing its effect on the radiative budget, we examine the thermal and hydrological responses to the radiative perturbation. We then explore the linearity of the climate response to cloud seeding by comparing the results of simulations with different geographical seeding areas. We conclude by discussing the implications of our results.

2. Methodology

We use a modified version of the Geophysical Fluid Dynamics Laboratory (GFDL) AM2.1 AGCM [*The GFDL Global Atmospheric Model Development Team*, 2004] to evaluate the top-of-atmosphere (TOA) radiative imbalances caused by cloud seeding. The AGCM features a prognostic scheme of N_d that allows for explicit consideration of the size distributions and chemical compositions of multiple aerosol types including sea salt [*Ming et al.*, 2006, 2007]. We then couple the AGCM to a mixed-layer ocean model to simulate the resulting equilibrium climate response. A detailed description of the coupled model configuration can be found in *Ming and Ramaswamy* [2009]. Results are taken over the last 20 years of the 80-year coupled mixed-layer ocean-AGCM simulation. In order to reliably discern the signal forced by cloud seeding from the climate system's natural variability, we calculate statistical significance by applying Student's t test at the 95% confidence level. All discussions of statistical significance refer to this criterion.

In this model, atmospheric sea salt concentrations are prescribed as a function of the satellite-retrieved surface wind speed [*Haywood et al.*, 1999]. We simulate cloud seeding by increasing sea salt aerosol concentrations fivefold for all size bins below the 850 hPa level within three regions located in the subtropical North Pacific (NP), South Pacific (SP), and South Atlantic (SA) (boxed regions in Fig. 1). These climatological subsidence regions are covered by persistent low level clouds and have relatively low aerosol burdens. Since cloud albedo change scales better with the fractional N_d change than the absolute change, the subtropical stratocumulus clouds have been identified previously as being particularly susceptible to seeding [*Latham et al.*, 2008]. The locations of the three seeding regions are similar to those used in J09 (Fig. 1 of J09), though ours cover nearly twice as much total area (Table 1). In addition to one non-seeded control run (CONT) and one run in which all three regions are seeded simultaneously (ALL) are three individual region runs in which only one of the three regions is seeded (NP, SP, and SA).

We keep fixed the levels of greenhouse gases and aerosol species (other than the aforementioned changes to sea salt) at pre-industrial (PI) levels. This choice makes it feasible to isolate the impacts of cloud seeding on the climate. By imposing cloud seeding as the sole perturbation to an otherwise equilibrium state, we can confidently attribute any simulated changes to seeding, rather than needing to untangle the confounding effects of seeding and greenhouse gas forcing. The linearity (or lack thereof) of the combined response to both perturbations will be addressed in a future study.

3. Results

3.1. Radiative flux perturbation

We quantify the effects of cloud seeding on the radiative budget in terms of radiative flux perturbation (RFP) [*Haywood et al.*, 2009]. That is, in the AGCM-only run we allow the entire atmosphere and land to respond to the injected aerosols while keeping sea surface temperatures (SST) fixed, and then take the TOA radiative flux difference between perturbation and control runs. RFP has been shown to be a good predictor of the resulting change in the surface temperature [*Ming et al.*, 2010; *Persad et al.*, 2012] and is a feasible way to quantify the aerosol indirect effects [*Lohmann et al.*, 2010].

The injected sea salt aerosols produce strong radiative deficits over the seeding regions. The mean in-region RFP is -8.5 W m^{-2}, and the global-mean is -0.73 W m^{-2}. The mean RFP over non-seeded areas is -0.20 W m^{-2}, which is statistically insignificant, indicating that the radiative effects of cloud seeding are mostly confined locally. This is consistent with the lack of clear spatial signal outside of the seeding regions (Fig. 1).

Decomposing the all-sky RFP into clear- and cloudy-sky components sheds additional light on how the added sea salt affects the system. The clear-sky component captures any direct scattering of sunlight by the added particles, while cloudy-sky RFP measures the aerosol indirect effects (note that this would not hold if the aerosols were absorptive instead of scattering; see *Persad et al.* [2012]). Global-mean clear- and cloudy-sky RFP in ALL are -0.41 and -0.32 W m^{-2}, respectively. Thus, over half of the radiative effect of seeding comes from direct scattering by the added sea salt. This is particularly significant given that, by specifying N_d directly, prior studies of the climate response to cloud seeding such as J09 and R09 do not capture this direct scattering component. The remaining RFP stems from the injected aerosol's microphysical effect on clouds. Averaged over all three seeding regions, N_d increases by 2.1 times over its control values, from 69 cm^{-3} in CONT to 148 cm^{-3} in ALL at the levels between 850-925 hPa (Table 1).

In each region, RFP is weakest nearest neighboring continental landmasses (Fig. 1) due to two factors. First, like many others, this AGCM is known to under-represent marine stratocumulus decks near land [*The GFDL Global Atmospheric Model Development Team*, 2004]. As such, cloudy-sky RFP and thus all-sky RFP are likely underestimated for all perturbation runs. Second, higher baseline aerosol concentrations near land cause N_d to be higher there in CONT. Thus, the fractional increase in N_d (and therefore absolute increase in cloud albedo) is less than in cleaner conditions farther out to sea.

3.2. Changes in temperature

We now consider the response of the coupled mixed-layer ocean-AGCM to the RFP, beginning with surface temperature. Despite the highly localized RFP, temperature responds in ALL relatively evenly over most of the globe (Fig. 2). It is known that the tropical free troposphere cannot sustain strong temperature gradients [e.g. *Sobel et al.*, 2001; *Kang et al.*, 2009]. Due to the tight convective coupling between the surface and the free troposphere, this argument of weak temperature gradient also holds for the surface, albeit to a lesser extent than in the free troposphere. Thus, cooling beneath the brightened clouds is bound to be re-distributed through the rest of the tropics. The cooling also extends to the mid- and high-latitudes, with the notable exception of the rather strong warming over the North Pacific, which will be discussed below.

Global-mean temperature change (δT) from CONT to ALL is -0.53 K, resulting in a climate sensitivity is 0.72 K m^2 W^{-1}. This is 65% (81%) of the sensitivity of an experiment performed with the same coupled model, but forced with PI to present-day anthropogenic GHG (aerosol) forcing [*Ming and Ramaswamy*, 2009]. The relatively low sensitivity to cloud seeding is likely partly due to seeding being highly localized in the tropics, compared to the globally uniform GHG or mid-latitude anthropogenic aerosols.

Though relatively smooth, the temperature response is not spatially homogeneous. As two of the seeding areas are over the eastern tropical Pacific, the equatorial Pacific cools more in the east than in the west (Fig. 2). This enhances the climatological equatorial SST gradient, thereby strengthening the Walker circulation. The annual-mean 300-hPa zonal winds over the equatorial Pacific become more westerly, while near-surface winds become more easterly. Thus, seeding has shifted the tropical Pacific to a La Niña-like state. The strengthening of the Walker circulation is consistent both with this La Niña-like response and with the decrease in global-mean temperature, which tends to enhance the tropical circulation based on a thermodynamic argument [*Ming et al.*, 2010]. This large-scale circulation change does not occur in all individual region runs and profoundly alters the regional precipitation patterns, as detailed in the subsequent sections.

As previously noted, much of the North Pacific warms, which is striking in light of the pronounced cooling virtually everywhere else. Directly adjacent sits a region of exceptionally strong cooling, centered over northwestern Canada (Fig. 2). This dipole pattern is a characteristic of the Pacific-North America oscillation (PNA), a large-scale climate variability mode [e.g. *Horel and Wallace*, 1981]. It has been shown that PNA is correlated with ENSO – the negative (positive) PNA phase with La Niña (El Niño) [*Horel and Wallace*, 1981]. 500-hPa geopotential heights in ALL are anomalously high in the North Pacific and low over Alaska and northwestern Canada, resembling the negative phase of PNA. Thus, the seemingly spurious region of warming appears to stem from the La Niña-like tropical condition caused by the preferential cooling of the equatorial East Pacific. A similar temperature dipole occurs in the ALL simulation of J09 (Fig. 3 of J09) and in both the 20% and 70% simulations in R09 (Fig. 1 of R09), all three of which also feature seeding over the subtropical South Pacific.

3.3. Changes in precipitation

The response of precipitation to cloud seeding depends simultaneously on multiple factors, including the global-mean δT and changes to SST patterns in both the Pacific and Atlantic. The global-mean precipitation change (δP) is -1.2% (-0.035 mm day^{-1}), which is relatively small, as the global-mean precipitation is tightly controlled by the atmospheric energy balance [*Allen and Ingram*, 2002]. The so called hydrological sensitivity (i.e. the global-mean δP divided by the global-mean δT) is 2.2% K^{-1}.

The tropical precipitation changes closely resemble climatological precipitation anomalies due to La Niña events (Fig. 2). Specifically, rainfall decreases across the central and eastern equatorial Pacific, while a dipole pattern in rainfall emerges in the western equatorial Pacific. Rainfall increases strongly over the maritime continent but decreases significantly directly northeast. A similar dipole pattern occurs in vertical velocity, ω.

This indicates an increased tropical overturning circulation. Interestingly, despite the clear negative phase PNA temperature pattern, no PNA-like trend occurs in precipitation. δP over the North Pacific and Alaska – modest decreases interspersed with statistically insignificant changes – is typical of most mid- to high-latitude regions.

The precipitation response over the Amazon Rainforest, given its importance ecologically and to the carbon cycle, is particularly critical to understand. The need becomes even more acute in light of the starkly differing responses to cloud seeding in model studies to date. In J09, precipitation decreased sharply over much of the Amazon (Fig. 4(b) of J09). However, J09 used a model unique amongst current-generation GCMs in that the Amazon dries out almost completely in global warming simulations [*Cox et al.*, 2008; *Harris et al.*, 2008]. This model bias likely accounts for some of the precipitation reductions. In contrast, rainfall increased moderately there in R09 (Fig. 3 of R09).

Meanwhile, most of the precipitation response in our ALL simulation over the Amazon is not statistically significant (Fig. 2). Multiple opposing factors are at play. On the one hand, the La Niña-like tropical precipitation response likely acts to increase rainfall over the Amazon [*Foley et al.*, 2002]. On the other hand, rainfall over the Amazon depends also on SST patterns in the tropical Atlantic. The tropical Atlantic cools more in the south than in the north, a pattern that has been shown to enhance subsidence over the Amazon [*Fu et al.*, 2001]. As an additional consideration, the global-mean temperature decrease also acts to decrease precipitation overall.

3.4. Nonlinearity with respect to the seeding regions

The temperature response varies significantly among the individual region runs and does not scale linearly with global-mean RFP for each run. Mean in-region RFP for NP, SP, and SA are -9.5, -8.7, and -7.3 W m^{-2}, respectively. The corresponding global-mean RFP values are -0.36, -0.41, and -0.31 W m^{-2} (Table 1). Global-mean δT values for NP, SP, and SA are -0.15, -0.42, and -0.06 K, respectively. Thus the SP region is the most potent at reducing the global-mean temperature, while SA has an almost negligible effect. This is borne out in their respective climate sensitivities (Table 1). The resulting linear sum of global-mean δT for NP, SP, and SA (the SUM case) is -0.63K, which is 19% greater than that of ALL. J09 ran analogous individual region simulations, obtaining similar results, including the relative strength (weakness) of SP (SA) in reducing global-mean temperature and a similar degree of nonlinearity in global-mean temperature change in their ALL vs. SUM experiments.

Analyzing the zonal-mean temperature changes helps shed further light on the nonlinearity (Fig. 3). All three individual region runs diverge substantially from ALL in the northern high latitudes, adding up to a temperature spike in SUM near 70°N. So whereas zonal-mean temperature in SUM is less than or equal to that of ALL at nearly all latitudes south of 50°N, SUM is warmer than ALL north of 50°N. This means that cooling is somehow enhanced in the northern high latitudes in ALL compared to SUM. Surface albedo feedback, often invoked as an important nonlinear phenomenon near the poles, does not play a major role in this nonlinearity, as fractional change in global-mean surface albedo in SUM and ALL are nearly the same (0.7% and 0.8% respectively).

The temperature response over the tropical Pacific varies among the different runs. In SP, the equatorial Pacific zonal SST gradient is enhanced similarly to ALL, thereby likewise triggering a La Niña-like precipitation response. In contrast, much of the temperature change is not statistically significant for the central and western equatorial Pacific in NP and for the eastern tropical Pacific in SA. As such, little can be said about the effects of seeding in NP and SA on the equatorial Pacific SST gradient. In light of this, we note that neither of these runs' climate responses appears at all La-Niña-like.

In the individual region runs of J09, only SA caused significant rainfall reduction in Amazonia. In all of our individual region runs including SA, the rainfall changes over the Amazon are statistically insignificant. One might expect Amazonian rainfall to be highly sensitive to seeding in SA, given the aforementioned role of the Atlantic meridional SST gradient. But unlike in ALL, little can be said about the role of this gradient in SA, as δT in the tropical north Atlantic is mostly statistically insignificant.

The individual region simulations suggest that climate response does not depend solely on global-mean RFP; rather, both the magnitude of RFP and its geographical location are critical. In particular, the climate is about 5 times more sensitive to the forcing over SP than to the one over SA (Table 1). It has been shown that the anomalous flow caused by an external forcing, at least to the first order, conforms to the climatological circulation [*Vecchi and Soden*, 2007]. Also, the bulk of the tropical circulation occurs in the Pacific. This could mean that the impact of a forcing over SP is more likely to be felt outside the seeding region through adjusting the circulation than a forcing of similar magnitude located over SA. On another note, global-mean temperature is observed to correlate strongly with the phase of the El Nino-Southern Oscillation (ENSO) [*Trenberth et al.*, 2002; *Foster and Rahmstorf*, 2011]. This appears consistent with our model results, in that the SST variation over the eastern equatorial Pacific can influence the global-mean δT. However, one has to interpret this with caution in light of the different time scales.

4. Discussion

Both our study and J09 demonstrate that the eastern equatorial Pacific is a very effective seeding region in terms of the magnitude of δT. Furthermore, we have demonstrated that seeding there directly alters the equatorial Pacific SST gradient that lies at the heart of the tropical dynamics. This presents a conundrum for any would-be geoengineers: the region in which cloud seeding would most effectively mitigate global-mean temperature rise is also a region in which seeding would very likely produce intense regional climate changes elsewhere.

Constraining the climate response to cloud seeding at regional scales using GCMs is complicated by model idiosyncracies, such as the drying out of the Amazon in the model used by J09 and the lack of marine low clouds near continents in the present study. However, several features, such as the dynamical constraint in the tropics on SST gradients, the thermodynamic constraints on global-mean δP and tropical circulation, and the sensitivity of the climate to equatorial Pacific SSTs, are well-established theoretical results that should be robust across GCMs. They therefore provide good starting points for constraining the climate response to cloud seeding.

Acknowledgments. We thank Tim Merlis and Caroline Muller for their thorough reviews. S.H. was partly supported by the NOAA Ernest F. Hollings Scholarship Program.

References

Allen, M. R., and W. J. Ingram (2002), Constraints on future changes in the hydrological cycle, *Nature*, *419*, 224–228.

Cox, P. M., P. P. Harris, C. Huntingford, R. A. Betts, M. Collins, C. D. Jones, T. E. Jupp, J. A. Marengo, and C. A. Nobre (2008), Increasing risk of Amazonian drought due to decreasing aerosol pollution, *Nature*, *453*, 212–216, doi:10.1038/nature06960.

Foley, J. A., A. Botta, M. T. Coe, and M. H. Costa (2002), El Niño-Southern oscillation and the climate, ecosystems and rivers of Amazonia, *Global Biogeochem. Cycles*, *16*, 1132–1151, doi:10.1029/2002GB001872.

Foster, G., and S. Rahmstorf (2011), Global temperature evolution 1979-2010, *Environ. Res. Lett.*, *6*, doi:10.1088/1748-9326/6/4/044022.

Fu, R., R. E. Dickinson, M. X. chen, and H. Wang (2001), How do tropical sea surface temperatures influence the seasonal distribution of precipitation in the equatorial Amazon?, *J. Climate*, *14*, 4003–4026.

Harris, P. P., C. Huntingford, and P. M. Cox (2008), Amazon Basin climate under global warming: the role of sea surface temperature, *Phil. Trans. R. Soc. B.*, *363*, 1753–1759.

Haywood, J. M., V. Ramaswamy, and B. J. Soden (1999), Tropospheric aerosol climate forcing in clear-sky satellite observations over the oceans, *Science*, *283*, 1299–1303.

Haywood, J. M., L. J. Donner, A. Jones, and J.-C. Golaz (2009), Global indirect radiative forcing caused by aerosols: IPCC (2007) and beyond, in *Clouds in the Perturbed Climate System*, edited by J. Heintzenberg and R. Charlson, MIT Press, Cambridge, MA, USA.

Horel, J. D., and J. M. Wallace (1981), Planetary scale atmospheric phenomena associated with the Southern Oscillation, *Mon. Weather Rev.*, *109*, 813–829.

Jones, A., J. Haywood, and O. Boucher (2009), Climate impacts of geoengineering marine stratocumulus clouds, *J. Geophys. Res.*, *114*, doi:10.1029/2008JD011450.

Kang, S. M., D. M. W. Frierson, and I. Held (2009), The tropical response to extratropical thermal forcing in an idealized gcm: The importance of radiative feedbacks and convective parameterization, *J. Atmos Sci*, *66*, doi:10.1175/2009JAS2924.1.

Latham, J. (1990), Control of global warming?, *Nature*, *347*, 339–340.

Latham, J. (2002), Amelioration of global warming by controlled enhancement of the albedo and longevity of low-level maritime clouds, *Atmos. Sci. Lett.*, *3*, 52–58.

Latham, J., P. Rasch, C. C. Chen, L. Kettles, A. Gadian, A. Gettelman, H. Morrison, K. Bower, and T. Choularton (2008), Global temperature stabilization via controlled albedo enhancement of low-level maritime clouds, *Phil. Trans. R. Soc. A*, *366*, 3969–3987, doi:10.1098/rsta.2008.0137.

Lohmann, U., L. Rotstayn, T. Storelvmo, A. Jones, S. Menon, J. Quaas, A. Ekman, D. Koch, and R. Ruedy (2010), Total aerosol effect: radiative forcing or radiative flux perturbation?, *Atmos. Chem. Phys.*, *10*, 3235–3246.

Ming, Y., and V. Ramaswamy (2009), Nonlinear climate and hydrological responses to aerosol effects, *J. Climate*, *22*, 1329–1339.

Ming, Y., V. Ramaswamy, L. J. Donner, and V. T. J. Phillips (2006), A new parameterization of cloud droplet activation applicable to general circulation models, *J. Atmos. Sci.*, *63*, 1348–1356.

Ming, Y., V. Ramaswamy, L. J. Donner, V. T. J. Phillips, S. A. Klein, P. A. Ginoux, , and L. W. Horowitz (2007), Modeling the interactions between aerosols and liquid water clouds with a self-consistent cloud scheme in a general circulation model, *J. Atmos. Sci.*, *64*, 1189–1209.

Ming, Y., V. Ramaswamy, and G. Persad (2010), Two opposing effects of absorbing aerosols on global-mean precipitation, *Geophys. Res. Lett.*, *37*, L13,701.

Persad, G., Y. Ming, and V. Ramaswamy (2012), Robust tropical tropospheric responses to absorbing aerosols, *J. Climate*, *25*, 2471–2480, doi:10.1175/JCLI-D-11-00122.1.

Rasch, P. J., J. Latham, and C. C. Chen (2009), Geoengineering by cloud seeding: influence on sea ice and climate system, *Environ. Res. Lett.*, *4*.

Sobel, A. H., J. Nilsson, and L. M. Polvani (2001), The weak temperature gradient approximation and balanced tropical moisture waves, *J. Atmos. Sci*, *58*, 3650–3665.

The GFDL Global Atmospheric Model Development Team (2004), The new GFDL global atmosphere and land model AM2-LM2: Evaluation with prescribed SST simulations, *J. Climate*, *17*, 4641–4673.

Trenberth, K. E., J. M. Caron, D. P. Stepaniak, and S. Worley (2002), Evolution of El Niño-Southern Oscillation and global atmospheric temperatures, *J. Geophys. Res.*, *107*, 4065–4081, doi:10.1029/2000JD000298.

Vecchi, G. A., and B. J. Soden (2007), Global warming and the weakening of the tropical circulation, *J. Climate*, *20*, 4316–4340, doi:10.1175/JCLI4258.1.

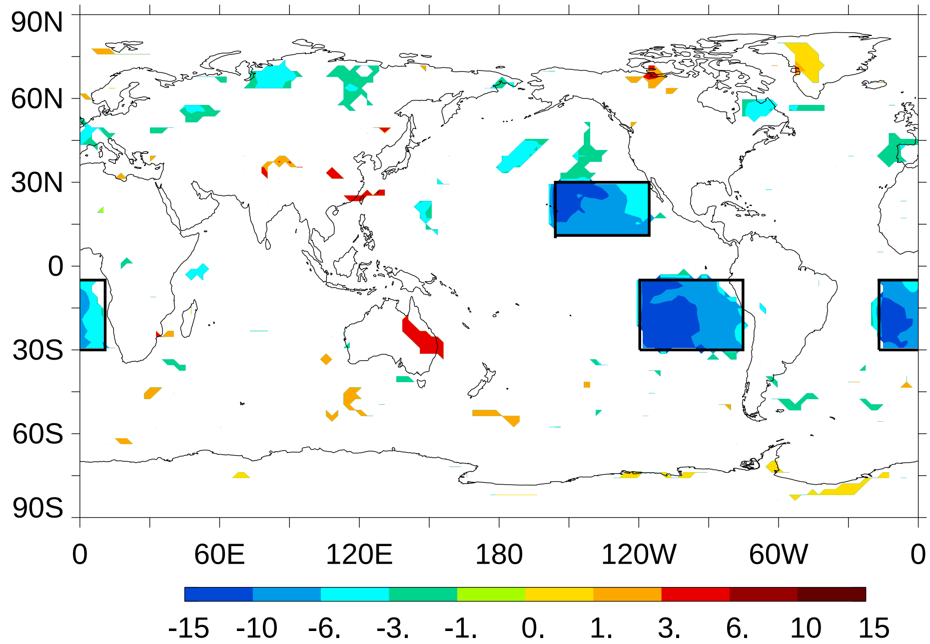

Figure 1. Annual-mean radiative flux perturbation (W m^{-2}) in ALL. Areas shaded white are not statistically significant at the 95% confidence level. The three seeding regions, located in the subtropical North Pacific (NP), South Pacific (SP), and South Atlantic (SA), are boxed. Only the ocean portion of the SP box is seeded.

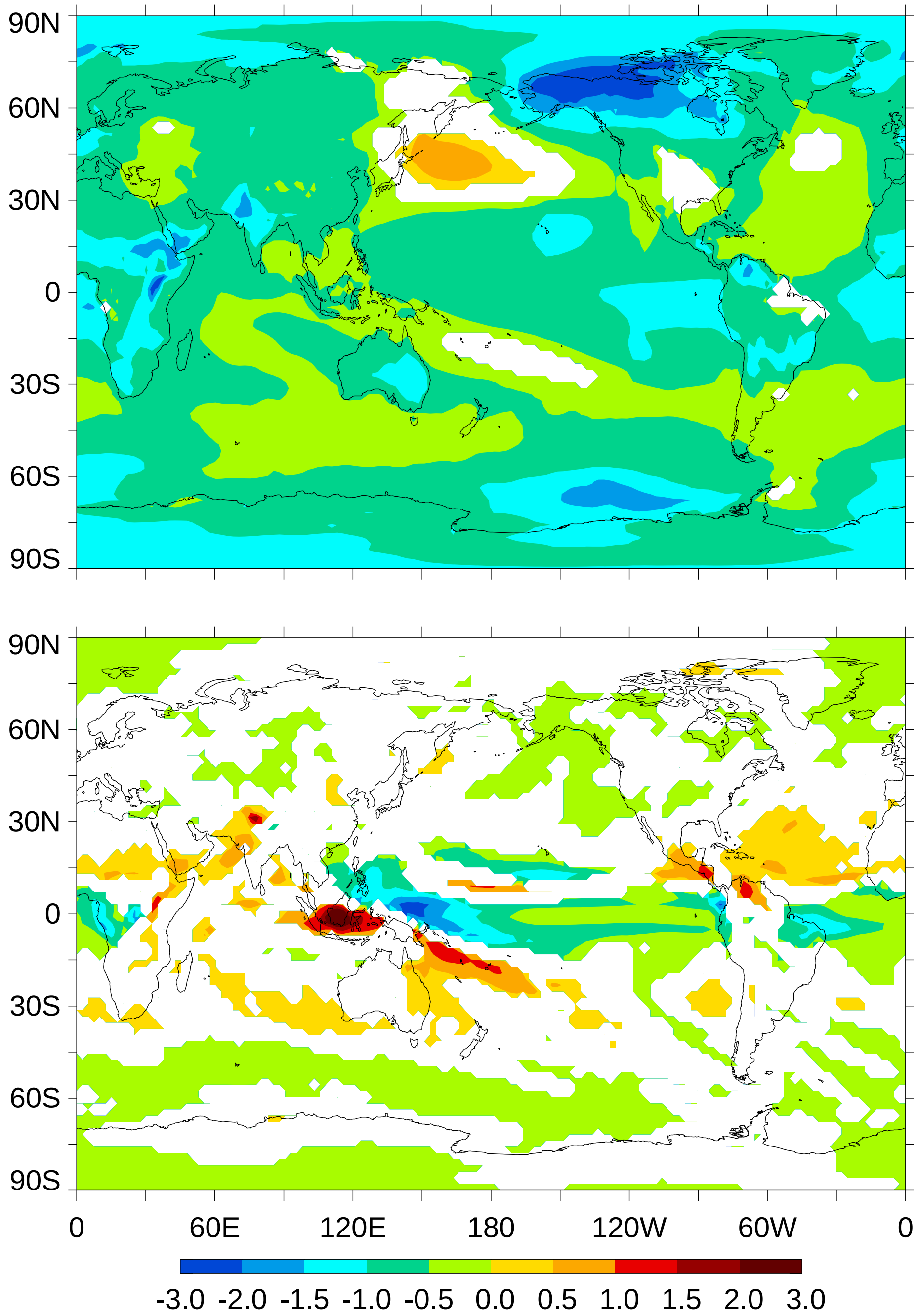

Figure 2. Annual-mean changes in (top) surface temperature (K) and (bottom) precipitation (mm day^{-1}) in ALL. Areas shaded white are not statistically significant at the 95% confidence level.

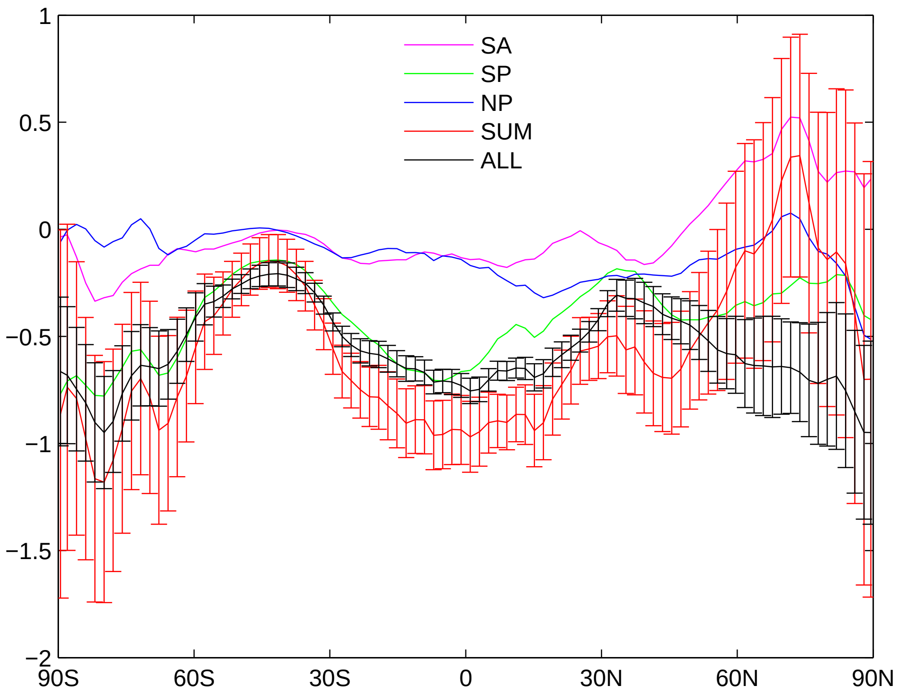

Figure 3. Zonal-mean changes in surface temperature (K) in SA, SP, NP, the linear sum of SA+SP+NP (SUM), and ALL. Error bars on SUM and ALL denote 95% confidence intervals.

Table 1. Surface area for each seeding region (% of the total earth surface area), mean fractional change in N_d within the seeding region(s) between 850-1000 hPa, mean RFP within the seeding region(s) (W m^{-2}), global-mean RFP (W m^{-2}), global-mean δT (K), and climate sensitivity λ (K m^2 W^{-1}). The δT and λ values in parentheses in ALL are for SUM; SUM and ALL are identical in all other categories.

Run	Area	δN_d	In-Region RFP	Global-mean RFP	δT	λ
ALL	6.4	2.1	-8.5	-0.73	-0.53 (-0.63)	0.73 (0.86)
NP	1.9	2.5	-8.8	-0.36	-0.15	0.42
SP	2.6	2.1	-8.8	-0.41	-0.42	1.02
SA	1.8	1.9	-7.2	-0.31	-0.06	0.19